Predictive Control of a 27-level Asymmetric Multilevel Current Source Inverter

Javier Muñoz, Bairon Soto, Ariel Villalón, Marco Rivera
Department of Electrical Engineering
Universidad de Talca
Curicó, Chile
jamunoz@utalca.cl

Pablo Cossutta, Miguel Aguirre
CIDEI - ITBA
Instituto Tecnológico de Buenos Aires
Buenos Aires, Argentina
pcossutt@itba.edu.ar

***Abstract*—In this work a study of a 27-level asymmetric multilevel current source inverter is developed. The presented structure is composed by three current source inverters that together are in a 9:3:1 ratio to produce a current waveform with multiple levels. A model predictive control scheme is developed for tracking the references for the output AC voltages, and to keep the asymmetric ratio between the DC currents even during transient conditions. Furthermore, an extra control goal is included in order to reduce the commutations of the inverter, and therefore reduce the power losses. In order to apply the predictive controller, the equations of the model to be analyzed are obtained systematically for continuous and discrete time domains. Simulations are carried out to validate the proposal and the integrity of the predictive control strategy.**

***Keywords*—Predictive Control, Asymmetric Multilevel Inverter, Current Source Inverter.**

I. Introduction

Multilevel converters have been of great importance the last years due to the increase on demand for clean, reliable, and economically feasible energy. Thus, systems that can maximize the efficient delivery of energy are required [1]. These devices have the capability of converting energy from DC to AC, an essential requirement for embedding renewable energy into existing power systems [2].

Since there must be power balance between components of multilevel converters, control algorithms may become complex [3]–[5]. As an alternative to decrease the number of converters in a multilevel topology, and therefore simplifying the control strategies, asymmetric multilevel inverters appear as a very promising and convenient option [6], [7]. They can reach the same levels of commutation with lower quantity of modules, aspect that reduces substantially the amount of states to commutate, making simpler the implementation of a control algorithm [8].

Regarding the control strategy used in this paper, a Model Predictive Control (MPC) is considered to track the AC voltages and to regulate the DC currents. Also, an additional term is added to the cost function in order to reduce the commutation losses, which can be done thanks to the flexibility of the MPC [9]–[13].

This work was supported by the Chilean Government under Project CONICYT/FONDECYT/1160806.

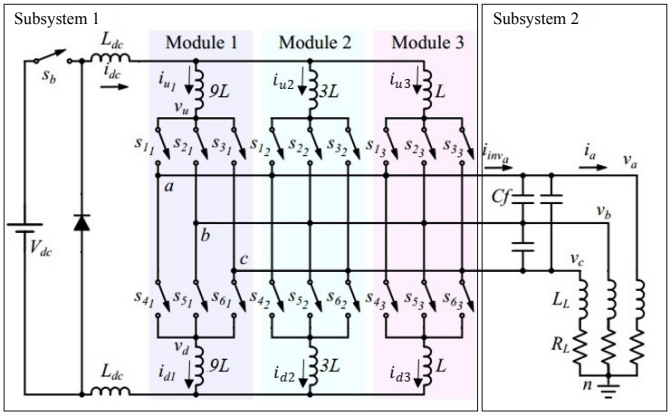

Fig. 1: Topology of the Asymmetric Multilevel Current Source Inverter (AMCSI)

In the present work, a 27-level Asymmetric Multilevel Current Source Inverter (AMCSI) is developed considering three modules with a 9:3:1 ratio. A predictive control scheme is used to control the inverter and the simulation results are included for strengthening the proposal.

II. System Modeling

A. The Asymmetric Topology

The topology of the asymmetric multilevel inverter developed in this work is shown in Fig.1 and has the following components: a voltage source, a buck converter and three current source inverters that are connected to a three-phase RLC load, where the role of passive filtering is played by the capacitors in order to smooth the voltage waveform out. The modules that are part of the AMCSI are parallel connected and their respective inductances are in the 9:3:1 ratio ($9L$, $3L$, and L). With this is possible to have the same asymmetry between the current of the inverters. A DC current i_{dc} feeds both inverters with an inductance L_{dc}.

A current waveform of up to 27 levels can be generated with this asymmetrical relation as explained in [14]. It is relevant to mention that if the symmetric approach is considered to generate the same number of levels, 13 inverters are required, increasing considerably thus the complexity of the model

TABLE I: AC currents and voltage v_{ud} for module j

State	s_{1_j}	s_{2_j}	s_{3_j}	s_{4_j}	s_{5_j}	s_{6_j}	i_{a_j}	i_{b_j}	i_{c_j}	v_{ud_j}
#1	1	0	0	1	0	0	$i_{u_j} - i_{d_j}$	0	0	0
#2	1	0	0	0	1	0	i_{u_j}	$-i_{d_j}$	0	v_{ab}
#3	1	0	0	0	0	1	i_{u_j}	0	$-i_{d_j}$	v_{ac}
#4	0	1	0	1	0	0	$-i_{d_j}$	i_{u_j}	0	v_{ba}
#5	0	1	0	0	1	0	0	$i_{u_j} - i_{d_j}$	0	0
#6	0	1	0	0	0	1	0	i_{u_j}	$-i_{d_j}$	v_{bc}
#7	0	0	1	1	0	0	$-i_{d_j}$	0	i_{u_j}	v_{ca}
#8	0	0	1	0	1	0	0	$-i_{d_j}$	i_{u_j}	v_{cb}
#9	0	0	1	0	0	1	0	0	$i_{u_j} - i_{d_j}$	0

predictive control (MPC) strategy, because the high number of switching states.

B. Continuous-Time Model

To represent the system as well as its valid states for the predictive control strategy, mathematical equations are required. These equations anticipate the behavior of the variables to be controlled as AC output voltages and DC currents. To each module to allow a valid circuit for the current, one of the upper switches and one of the lower switches have to be closed in all the inverters. This requirement is expressed in the following relation,

$$s_{1_j} + s_{2_j} + s_{3_j} = s_{4_j} + s_{5_j} + s_{6_j} = 1 \quad j \in \{1, 2, 3\} \tag{1}$$

where j is the number of the module.

As deeply explained in the technical literature [15], each current source inverter (CSI) has 9 valid switching states. As the AMCSI considers three modules with 9 active states each one to produce 27 levels, the number of possible combinations is given by $9^3 = 729$, which is quite lower than its symmetric counterpart equal to $9^{13} = 2.5 \cdot 10^{12}$ valid switching states. This is clearly unfeasible for any existing digital board such as DSP or FPGA. The latter leads to that for having high amount of levels in the multilevel waveform, the asymmetric approach has to be taken into account since it allows more levels than the symmetric multilevel inverter.

To obtain the model of the system in continuous-time mode, the valid states from Table I have to be used for modeling the current sources for each inverter (subsystem 1 from the Fig. 1), and for describing the dynamic load behavior, differential equations have to be modeled (subsystem 2 from the Fig. 1).

Therefore, applying Kirchhoff's laws, subsystem 1 model equations are obtained as follows,

$$\begin{cases} i_{dc} &= i_{u1} + i_{u2} + i_{u3} \\ i_{dc} &= i_{d1} + i_{d2} + i_{d3} \\ V_{dc} s_b &= 2L_{dc}\dot{i_{dc}} + 9L\dot{i_{u1}} + v_{un1} + v_{nd1} + 9L\dot{i_{d1}} \\ V_{dc} s_b &= 2L_{dc}\dot{i_{dc}} + 3L\dot{i_{u2}} + v_{un2} + v_{nd2} + 3L\dot{i_{d2}} \\ V_{dc} s_b &= 2L_{dc}\dot{i_{dc}} + L\dot{i_{u3}} + v_{un3} + v_{nd3} + L\dot{i_{d3}} \\ V_{dc} s_b &= 2L_{dc}\dot{i_{dc}} + 9L\dot{i_{u1}} + v_{un1} + v_{nd2} + 3L\dot{i_{d2}} \\ V_{dc} s_b &= 2L_{dc}\dot{i_{dc}} + 3L\dot{i_{u2}} + v_{un2} + v_{nd3} + L\dot{i_{d3}} \end{cases} \tag{2}$$

where s_b is the state of the buck converter switch that controls the current source.

In the first two equations in 2, i_{dc} appears linearly dependent on the currents from the current source inverters (CSIs). Consequently, the DC current can be formulated as i_{u_j} and i_{d_j}, implying that i_{dc} can no longer be considered to determine the future behavior of the system.

Whereas, the voltages among nodes u_j and n, and between n and d_j, v_{un_j} and v_{nd_j}, respectively, can be represented in terms of the commutation signals s_{1-6_j} according to the following expression,

$$\begin{aligned} \begin{bmatrix} v_{un_1} \\ v_{un_2} \\ v_{un_3} \end{bmatrix} &= \begin{bmatrix} s_{1_1} & s_{2_1} & s_{3_1} \\ s_{1_2} & s_{2_2} & s_{3_2} \\ s_{1_3} & s_{2_3} & s_{3_3} \end{bmatrix} \begin{bmatrix} v_a \\ v_b \\ v_c \end{bmatrix} \\ \begin{bmatrix} v_{nd_1} \\ v_{nd_2} \\ v_{nd_3} \end{bmatrix} &= - \begin{bmatrix} s_{4_1} & s_{5_1} & s_{6_1} \\ s_{4_2} & s_{5_2} & s_{6_2} \\ s_{4_3} & s_{5_3} & s_{6_3} \end{bmatrix} \begin{bmatrix} v_a \\ v_b \\ v_c \end{bmatrix} \end{aligned} \tag{3}$$

Similarly, the inverter output current i_{inv} for each phase follows what is shown in 4 considering the commutation signals s_{1-6_j} as,

$$\begin{bmatrix} i_{inv_a} \\ i_{inv_b} \\ i_{inv_c} \end{bmatrix} = \begin{bmatrix} s_{1_1} & s_{1_2} & s_{1_3} \\ s_{2_1} & s_{2_2} & s_{2_3} \\ s_{3_1} & s_{3_2} & s_{3_3} \end{bmatrix} \begin{bmatrix} i_{u_1} \\ i_{u_2} \\ i_{u_3} \end{bmatrix} - \begin{bmatrix} s_{4_1} & s_{4_2} & s_{4_3} \\ s_{5_1} & s_{5_2} & s_{5_3} \\ s_{6_1} & s_{6_2} & s_{6_3} \end{bmatrix} \begin{bmatrix} i_{d_1} \\ i_{d_2} \\ i_{d_3} \end{bmatrix} \tag{4}$$

Taking into account (2), (3) and (4), the overall model of subsystem 1 can be obtained as,

$$\begin{aligned} \begin{bmatrix} \dot{i}_{u_1} \\ \dot{i}_{u_2} \\ \dot{i}_{u_3} \\ \dot{i}_{d_1} \\ \dot{i}_{d_2} \\ \dot{i}_{d_3} \end{bmatrix} &= a \begin{bmatrix} -b & c & d & -3 & -9 & -27 \\ c & -e & f & -9 & -27 & -81 \\ d & f & -3g & -27 & -81 & -243 \\ -3 & -9 & -27 & -b & c & d \\ -9 & -27 & -81 & c & -e & f \\ -27 & -81 & -243 & d & f & -3g \end{bmatrix} \begin{bmatrix} v_{un_1} \\ v_{un_2} \\ v_{un_3} \\ v_{nd_1} \\ v_{nd_2} \\ v_{nd_3} \end{bmatrix} \\ &\quad + a\, s_b \begin{bmatrix} 39 \\ 117 \\ 351 \\ 39 \\ 117 \\ 351 \end{bmatrix} V_{dc} \end{aligned} \tag{5}$$

where,

$$\begin{aligned} a &= \frac{1}{78\,(9L + 13\,L_{dc})} & b &= 75 + 104\frac{L_{dc}}{L} \\ c &= 9 + 26\frac{L_{dc}}{L} & d &= 27 + 78\frac{L_{dc}}{L} \\ e &= 207 + 260\frac{L_{dc}}{L} & f &= 81 + 243\frac{L_{dc}}{L} \\ & & g &= 153 + 104\frac{L_{dc}}{L} \end{aligned} \tag{6}$$

The load and the passive output filter result in an equivalent RLC impedance seen from the converter output. Therefore, the model of the subsystem 2 is as follows,

$$\begin{cases} \dot{v_\eta} = \dfrac{i_{inv\eta} - i_\eta}{3\,C_f} \\ \dot{i_\eta} = \dfrac{v_\eta - R_L\,i_\eta}{L_L} \end{cases} \qquad \eta \in \{a,b,c\} \tag{7}$$

where L_L and R_L are the inductive and resistive values of the load, respectively; and C_f is the capacitance of the passive filter. The input of the subsystem 2 is i_{inv_η}, which corresponds to the output of the subsystem 1. As depicted in [16], the overall representation of this subsystem is,

$$\begin{bmatrix} \dot{v}_a \\ \dot{v}_b \\ \dot{v}_c \\ \dot{i}_a \\ \dot{i}_b \\ \dot{i}_c \end{bmatrix} = \begin{bmatrix} 0 & 0 & 0 & f & 0 & 0 \\ 0 & 0 & 0 & 0 & f & 0 \\ 0 & 0 & 0 & 0 & 0 & f \\ g & 0 & 0 & h & 0 & 0 \\ 0 & g & 0 & 0 & h & 0 \\ 0 & 0 & g & 0 & 0 & h \end{bmatrix} \begin{bmatrix} v_a \\ v_b \\ v_c \\ i_a \\ i_b \\ i_c \end{bmatrix} - f \begin{bmatrix} i_{inv_a} \\ i_{inv_b} \\ i_{inv_c} \\ 0 \\ 0 \\ 0 \end{bmatrix} \tag{8}$$

where,

$$f = -\frac{1}{3\,C_f} \qquad g = \frac{1}{L_L} \qquad h = \frac{R_L}{L_L} \tag{9}$$

C. Discrete-Time Model

In order to use a predictive control scheme, the dynamic model of the system needs to be expressed in discrete-time. Therefore, the equations have to be in a discrete representation, using the Euler approximation. This considers the derivative of an arbitrary variable x, which can be a voltage or current:

$$\frac{dx}{dt} = \frac{x_{k+1} - x_k}{T_s} \tag{10}$$

where T_s is the sampling time. Considering this approximation, the model (5) can be discretized, resulting the equation (11).

$$\begin{aligned} \begin{bmatrix} i_{u_1} \\ i_{u_2} \\ i_{u_3} \\ i_{d_1} \\ i_{d_2} \\ i_{d_3} \end{bmatrix}_{k+1} = aT_s \begin{bmatrix} -b & c & d & -3 & -9 & -27 \\ c & -e & f & -9 & -27 & -81 \\ d & f & -3g & -27 & -81 & -243 \\ -3 & -9 & -27 & -b & c & d \\ -9 & -27 & -81 & c & -e & f \\ -27 & -81 & -243 & d & f & -3g \end{bmatrix} \begin{bmatrix} v_{un_1} \\ v_{un_2} \\ v_{un_3} \\ v_{nd_1} \\ v_{nd_2} \\ v_{nd_3} \end{bmatrix}_k \\ + \begin{bmatrix} i_{u_1} \\ i_{u_2} \\ i_{u_3} \\ i_{d_1} \\ i_{d_2} \\ i_{d_3} \end{bmatrix}_k + aT_s s_b \begin{bmatrix} 39 \\ 117 \\ 351 \\ 39 \\ 117 \\ 351 \end{bmatrix} V_{dc} \end{aligned} \tag{11}$$

In the same way, using (8) and (10), the representation in discrete time of the subsystem 2 is,

$$\begin{bmatrix} v_a \\ v_b \\ v_c \\ i_a \\ i_b \\ i_c \end{bmatrix}_{k+1} = \begin{bmatrix} 0 & 0 & 0 & f' & 0 & 0 \\ 0 & 0 & 0 & 0 & f' & 0 \\ 0 & 0 & 0 & 0 & 0 & f' \\ g' & 0 & 0 & h' & 0 & 0 \\ 0 & g' & 0 & 0 & h' & 0 \\ 0 & 0 & g' & 0 & 0 & h' \end{bmatrix} \begin{bmatrix} v_a \\ v_b \\ v_c \\ i_a \\ i_b \\ i_c \end{bmatrix}_k - f' \begin{bmatrix} i_{inv_a} \\ i_{inv_b} \\ i_{inv_c} \\ 0 \\ 0 \\ 0 \end{bmatrix}_k \tag{12}$$

where,

$$f' = -\frac{T_s}{3\,C_f} \qquad g' = \frac{T_s}{L_L} \qquad h' = 1 - \frac{R_L}{L_L}\,T_s \tag{13}$$

III. Model predictive control strategy

Since the AMCSI has already 729 valid switching states due to the three modules, also the buck converter switch needs to be considered as it has other two possible switching states, adding another 729 states giving a total of 1,458 combinations. Thus, all the state variables and commutation switches predictions have to be calculated by the control strategy in order to minimize the global cost function.

On the other side, for taking into account the delay generated by the internal computing of the control, outputs obtained from the predictive control are applied to the $k+1$ sampling time. This foists the constraint of calculating in less than T_s seconds all the required predictions.

Additionally, the inverter currents in the $k+1$ sampling time depend on the switching states at the k time, thus only at the $k+2$ time, the load variables $v_{a,b,c}$ may be predicted. Any variation in the state at the k time will affect the load variables at the $k+2$ instant, as explained in [17].

For establishing the MPC scheme, a multi-variable cost function has to be defined to complete the predictive algorithm. In this, every possible combination at the $k+2$ time has to be considered and the minimum-cost state of the function to be chosen by the controller.

Through the reference current i_{dc}, individual references can be obtained for each module, with its respective asymmetric distribution, i.e. the currents i_{u1} and i_{d1} are equal to $\frac{9}{13}i_{dc_{ref}}$, i_{u2}, and i_{d2} are equal to $\frac{3}{13}i_{dc_{ref}}$ and i_{u3} with i_{d3} are established in $\frac{1}{13}i_{dc_{ref}}$. Thus, the expression of the cost associated to the reference currents is equal to,

$$\begin{aligned} c_{i_{dc1}} &= \left(i_{u_{1_{k+2}}} - \frac{9}{13}i_{dc_{ref}}\right)^2 + \left(i_{d_{1_{k+2}}} - \frac{9}{13}i_{dc_{ref}}\right)^2 \\ c_{i_{dc2}} &= \left(i_{u_{2_{k+2}}} - \frac{3}{13}i_{dc_{ref}}\right)^2 + \left(i_{d_{2_{k+2}}} - \frac{3}{13}i_{dc_{ref}}\right)^2 \\ c_{i_{dc3}} &= \left(i_{u_{2_{k+2}}} - \frac{1}{13}i_{dc_{ref}}\right)^2 + \left(i_{d_{2_{k+2}}} - \frac{1}{13}i_{dc_{ref}}\right)^2 \end{aligned} \tag{14}$$

On the other hand, the output voltages must be included in the load, which is why the sum of square errors compared to a voltage reference is developed.

$$\begin{aligned} c_{v_{ref}} = (v_{a_{k+2}} - v^*_{a_{k+2}})^2 + (v_{b_{k+2}} - v^*_{b_{k+2}})^2 \\ + (v_{c_{k+2}} - v^*_{c_{k+2}})^2 \end{aligned} \tag{15}$$

In order to find the voltage references as they are the known control system inputs at the k time, a prediction at the $k+2$ time has to be made. For this a fourth-order Lagrange extrapolation is used, which is given as follows,

$$v^*_{k+1} = 4v^*_k - 6v^*_{k-1} + 4v^*_{k-2} - v^*_{k-3} \tag{16}$$

While the references for the $k+2$ time are,

$$v^*_{k+2} = 10v^*_k - 20v^*_{k-1} + 15v^*_{k-2} - 4v^*_{k-3} \tag{17}$$

As explained in the related literature, since the sampling time is small enough and the signal follows a sine wave at the line frequency of the extrapolation, this estimation is able to be used for several frequencies of v^*.

Moreover, it is desirable diminishing the commutation frequency and improving the efficiency. These both together reduce the energy losses produced by such commutation. For this, a penalty term for the state transitions which produce the biggest number of changes in the commutation states within a certain sampling time is included.

The amount of changing-switches within each sampling time is given by,

$$N_{sw_j} = \sum_{i=1}^{6} \left| s_{i_{j_{k+1}}} - s_{i_{j_k}} \right| \quad j \in \{1,2,3\} \tag{18}$$

The cost function related to the commutation of the AMCSI and the buck converter follows the expression,

$$c_{sw} = \lambda_1 N_{sw_1} + \lambda_2 N_{sw_2} + \lambda_3 N_{sw_3} + \lambda_{buck} \left| s_{b_{k+1}} - s_{b_k} \right| \tag{19}$$

where, the $\lambda_{1,2,3}$ and λ_{buck} weighting factors are selected to accomplish the needed commutation frequency. Furthermore, a global weighting factor is applied to each component of the global cost function for normalizing them,

$$\lambda_{vref} = \frac{1}{e^2_{v_{ref}}} \qquad \lambda_{i_{dc}} = \frac{1}{e^2_{i_{dc}}} \tag{20}$$

where $e_{v_{ref}}$ and $e_{i_{dc}}$ are the desired error limits of the output voltage and current. Finally, the sum of the terms weighted by their factors leads to the global cost function,

$$c_{global} = \lambda_{v_{ref}} c_{v_{ref}} + \lambda_{i_{dc_1}} c_{i_{dc_1}} + \lambda_{i_{dc_2}} c_{i_{dc_2}} + \lambda_{i_{dc_3}} c_{i_{dc_3}} + c_{sw} \tag{21}$$

The commutation state that minimizes eq. (21) is selected and applied at the $k+1$ time.

IV. Simulation Results

The proposed control scheme is validated by simulations performed using MATLAB/Simulink. The simulations are implemented with the parameters shown in Table II. The prediction is carried out using a sampling time of $T_s = 200\ \mu s$.

The representative waveforms that show stationary performance of the system are shown in Fig. 2, where (a) corresponds to the output voltage that follows correctly its references; (b) represents the line-to-line voltage of v_{ab}. In

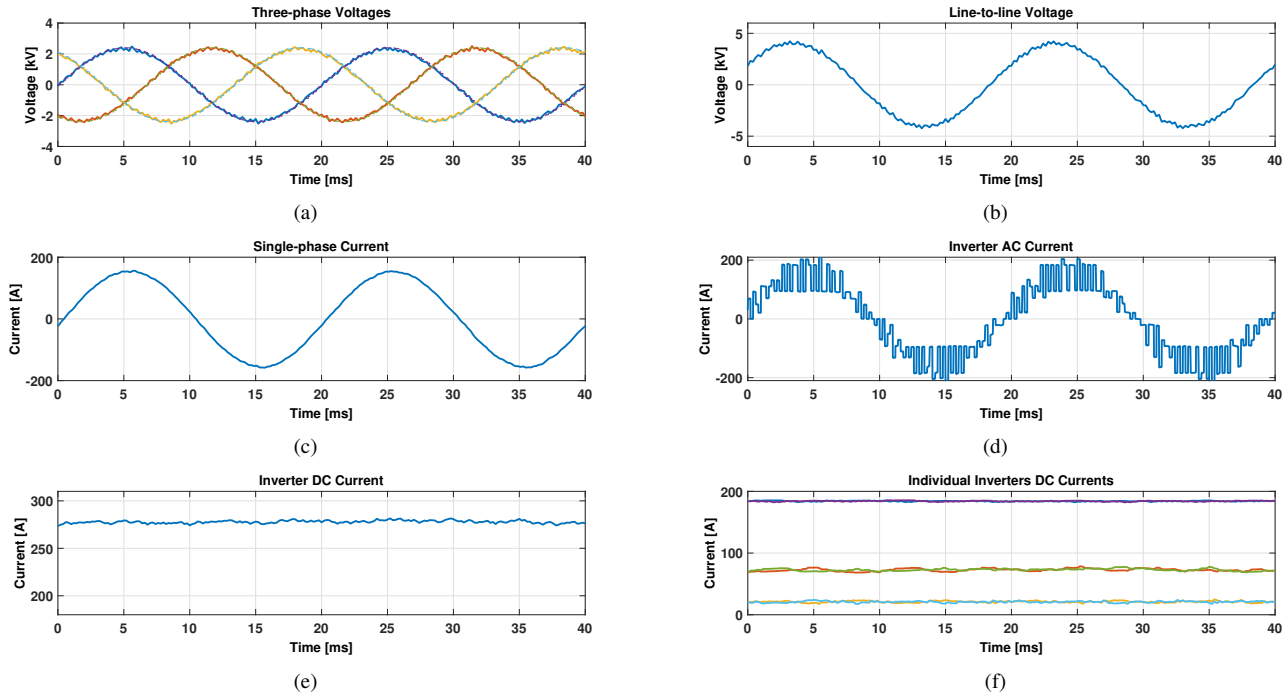

Fig. 2: Stationary results; (a) phase voltages and references, (b) line-to-line output voltage v_{ab}, (c) output current i_a, (d) inverter output current of phase a, (e) inductor current i_{dc}, (f) inverter asymmetric currents.

TABLE II: System parameters

Symbol	Definition	Value
V_{dc}	Voltage source	$5kV$
R_L	Load resistor	12Ω
L_L	Load inductor	$6mH$
L_{dc}	DC inductor	$120mH$
L	DC divider inductor base	$120mH$
C_f	Filter capacitors	$22.2\mu F$
T_s	Sampling time	$200\mu s$
f_l	Reference frequency	$50Hz$
$i_{dc_{ref}}$	Reference current	$270A$
v_{ref}	Reference voltage	$2.9kV$

(c) is seen that the load current i_a is highly sinusoidal, and that it is obtained with a low-frequency commutation, as shown in (d). The plot from (e) shows the DC current of the inverter, where it can be seen that the tracking of its reference value has a small error, since the predictive control is not able to eliminate it in the steady state, but only reducing it. Considering this last issue, in the graph from (f) the asymmetric distribution of currents which follows the 9:3:1 ratio with a small margin of error are shown.

In particular, the steady state error of the DC variables does not affect the performance of the controller in the AC variables; furthermore this error can be reduced by adjusting the weighting factors of the global cost function shown in (21).

Fig. 3 shows that THD of the current i_a is 1.13% which is relatively low because of the inclusion of the capacitive filters. On the other side, THD of I_{inv_a} is 26.9%, and 2.72% for V_{ab}. The THD results meet the expected values for such index; and therefore it is possible to mention that the implementation of the asymmetric inverter is feasible. Compared with the symmetric structure, with less possible combinations a higher number of levels is accomplished, as it will be shown in the forthcoming section.

Additionally, a 25% step-up voltage reference change was performed to assess the transient response of the proposed control algorithm; the main results are presented in Fig. 4. The proposed strategy achieves voltage reference tracking fast dynamics, as it can be seen in Fig. 4 (a). The line-to-line voltage v_{ab} is shown in Fig. 4 (b), where it is possible to observe that the reference change leads to an increment in this variable. In Fig. 4 (c) with a step-up change, a rise in the output current is implied, but it reaches its new operation condition smoothly. Finally, in Fig. 4 (d) the inverter output current is shown, where it can be recognized that for tracking the new reference value, more levels are used.

V. Comparison of Topologies

Compared values among a 5-level symmetric multilevel current source inverter (5-L SMCSI) [17] and a 7-level asymmetric multilevel current source inverter (7-L AMCSI) [15] are shown in Table III and compared with the one developed in this work: the 27-level asymmetric multilevel current source inverter (27L-AMCSI).

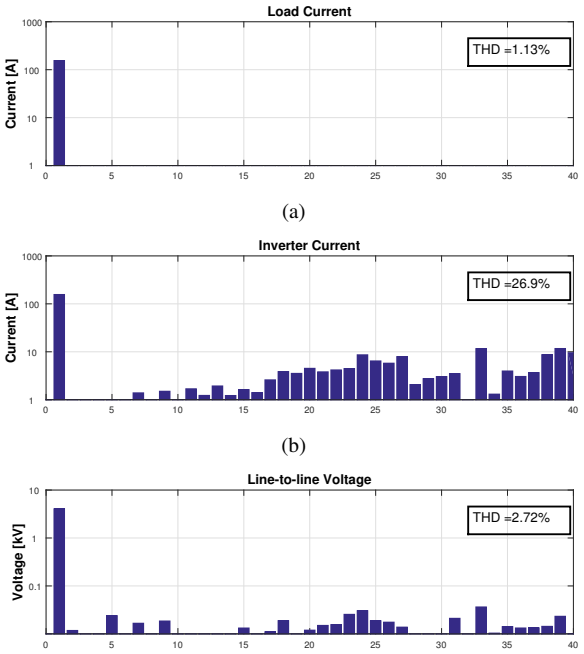

Fig. 3: Waveform spectrum versus harmonic order; (a) inverter output i_{inv_a}, (b) line-to-line output voltage v_{ab}, (c) output current i_a

The comparison among the amount of generated levels together with the valid states for each topology is made. The 27-levels topology presented in this paper has the same number of valid states of a five-states symmetric multilevel current source inverter due to the same number of converters connected in parallel.

Additionally, in Table III the compared numbers of semiconductors which need to be used for each topology are shown, together with the THD values for V_{ab}, I_{inv_a} and I_a.

With these THD values, it is possible to say that the proposed topology for the 27-levels AMCSI is a feasible technology prospect as it makes possible to generate 27 levels with lower number of commutation states that would be necessary for a symmetric multilevel current source inverter with the same number of levels.

TABLE III: Comparison among topologies

	5L-SMCSI	7L-AMCSI	27L-AMCSI
Levels	5	7	27
States	$9^3 = 729$	$9^2 = 81$	$9^3 = 729$
Semiconductors	18	12	18
THD V_{ab}	2.5%	3.01%	2.72%
THD I_{inv_a}	20.60%	19.86%	26.9%
THD I_a	1.20%	1.74%	1.13%

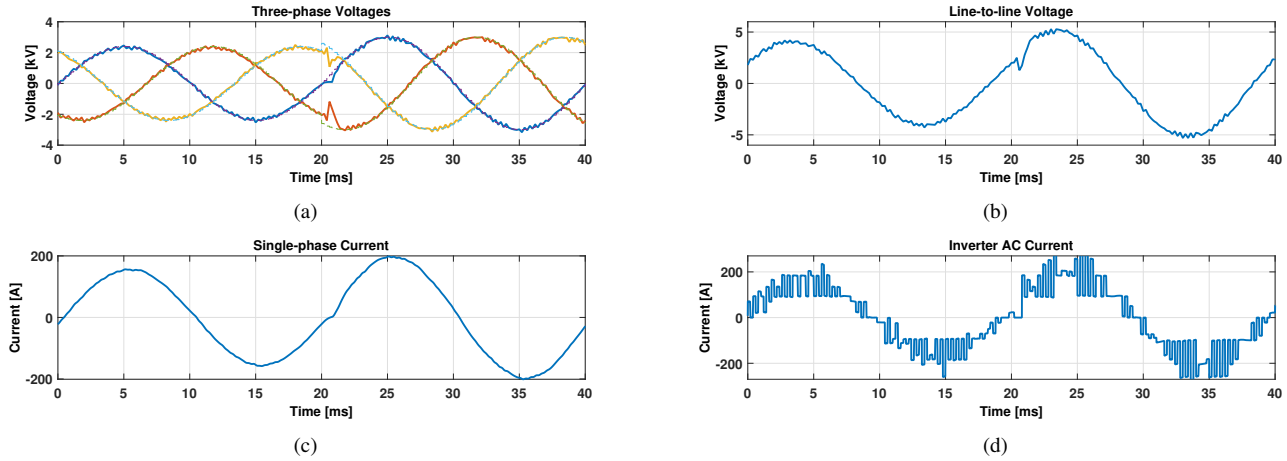

Fig. 4: Results for predictive control of the system with a step-change in voltage references; (a) phase voltages and references, (b) line-to-line output voltage v_{ab}, (c) output current i_a, (d) inverter output current of phase a [A]

VI. Conclusions

It is possible to generate a current waveform of up to 27 levels using only three modules, extensively reducing, thus, the number of possible commutations compared to the symmetric counterpart with the presented asymmetric multilevel current source inverter. This reduction of the possible commutations eases the implementation of the predictive control algorithm.

Although a simple cost function is presented, its efficacy is proved through the algorithm's good tracking of variables in steady state. In addition, an improvement of the efficiency of the entire system comes with the role of the controller, which balances the internal currents of the inverter and provides low switching frequency of the buck converter, reducing thus the switching losses.

Considering inside the controller the switching state of the buck converter leads to the option of using a non-constant power source while controlling the current that is fed to the AMCSI.

References

[1] C. O'Dwyer, L. Ryan, and D. Flynn, "Efficient large-scale energy storage dispatch: Challenges in future high renewable systems," *IEEE Transactions on Power Systems*, vol. 32, no. 5, pp. 3439–3450, Sept 2017.

[2] C. Chakraborty, H. H. C. Iu, and D. D.-C. Lu, "Power converters, control, and energy management for distributed generation," *IEEE Transactions on Industrial Electronics*, vol. 62, no. 7, pp. 4466–4470, July 2015.

[3] S. Mariethoz, "Design and control of high-performance modular hybrid asymmetrical cascade multilevel inverters," *IEEE Transactions on Industry Applications*, vol. 50, no. 6, pp. 4018–4027, 2014.

[4] Q.-C. Zhong and T. Hornik, *Control of Power Inverters in Renewable Energy and Smart Grid Integration*, 1st ed. West Sussex, United Kingdom: Wiley - IEEE Press, 2013. [Online]. Available: http://doi.wiley.com/10.1002/9781118481806

[5] J. Pereda and J. Dixon, "Cascaded multilevel converters: Optimal asymmetries and floating capacitor control," *IEEE Transactions on Industrial Electronics*, vol. 60, no. 11, pp. 4784–4793, 2013. [Online]. Available: https://ieeexplore.ieee.org/document/6339054/

[6] J. Muñoz, P. Gaisse, C. Baier, M. Rivera, R. Gregor, and P. Zanchetta, "Asymmetric multilevel topology for photovoltaic energy injection to microgrids," in *2016 IEEE 17th Workshop on Control and Modeling for Power Electronics, COMPEL 2016*. Trondheim, Norway: IEEE, 2016. [Online]. Available: https://ieeexplore.ieee.org/document/7556665/

[7] C. Dhanamjayulu and S. Meikandasivam, "Implementation and Comparison of Symmetric and Asymmetric Multilevel Inverters for Dynamic Loads," *IEEE Access*, vol. 6, pp. 738–746, 2018. [Online]. Available: http://ieeexplore.ieee.org/document/8186159/

[8] N. Mittal, B. Singh, S. Singh, R. Dixit, and D. Kumar, "Multilevel Inverters: A Literature Survey on Topologies and Control Strategies," in *Power, Control and Embedded Systems (ICPCES), 2012 2nd International Conference on*, Dec 2012, pp. 1–11.

[9] W. R. Sultana, S. K. Sahoo, S. Sukchai, S. Yamuna, and D. Venkatesh, "A review on state of art development of model predictive control for renewable energy applications," *Renewable and Sustainable Energy Reviews*, vol. 76, pp. 391 – 406, 2017.

[10] V. Yaramasu and B. Wu, *Fundamentals of Model Predictive Control*. Wiley-IEEE Press, 2017, pp. 512–.

[11] J. Rodriguez, J. Pontt, C. A. Silva, P. Correa, P. Lezana, P. Cortes, and U. Ammann, "Predictive Current Control of a Voltage Source Inverter," *IEEE Transactions on Industrial Electronics*, vol. 54, no. 1, pp. 495–503, 2007. [Online]. Available: http://ieeexplore.ieee.org/document/4084698/

[12] S. Vazquez, J. Rodriguez, M. Rivera, L. G. Franquelo, and M. Norambuena, "Model Predictive Control for Power Converters and Drives: Advances and Trends," *IEEE Transactions on Industrial Electronics*, vol. 64, no. 2, pp. 935–947, 2017.

[13] J. Rodríguez and P. Cortés, *Predictive Control of Power Converters and Electrical Drives*, 1st ed. Wiley - IEEE, 2012, p. 231.

[14] M. A. Perez, P. Cortes, and J. Rodríguez, "Predictive control algorithm technique for multilevel asymmetric cascaded H-bridge inverters," *IEEE Transactions on Industrial Electronics*, vol. 55, no. 12, pp. 4354–4361, 2008.

[15] P. Cossutta, M. Aguirre, J. Muñoz, M. Rivera, P. Melín, and J. Rohten, "7-level asymmetric multilevel current source inverter with predictive control," in *2017 IEEE 3rd Annual Southern Power Electronics Conference (SPEC)*, Dec 2017.

[16] P. Cossutta, M. P. Aguirre, A. Cao, S. Raffo, and M. I. Valla, "Single-Stage Fuel Cell to Grid Interface With Multilevel Current-Source Inverters," *IEEE Transactions on Industrial Electronics*, vol. 62, no. 8, pp. 5256–5264, Aug 2015.

[17] P. Cossutta, M. A. Engelhardt, M. Aguirre, J. Ponce, and M. I. Valla, "Model predictive control of a multilevel current source inverter together with its current source," in *ISIE 2017 - 26th IEEE International Symposium on Industrial Electronics*, Jun 2017.